JOURNAL OF THERMOPHYSICS AND HEAT TRANSFER
Vol. 20, No. 4, October–December 2006

Thermochemical Relaxation in Shock Tunnels

Chul Park*
Korea Advanced Institute of Science and Technology, Daejeon 305-701, Republic of Korea

DOI: 10.2514/1.22719

Thermochemical relaxation phenomena in the shock tunnel nozzle and behind a normal shock wave formed in its test section are investigated theoretically in one dimension using a state-to-state description. Test gas is assumed to be air containing hydrogen as an impurity. The state-to-state rate coefficients calculated by the forced harmonic oscillator model of Adamovich, Macheret, Rich, and Treanor ("Vibrational Energy Transfer Rates Using a Forced Harmonic Oscillator Model," Journal of Thermophysics and Heat Transfer, Vol. 12, No. 1, January–March 1998, pages 57-65) are multiplied by correction factors to numerically reproduce the existing experimental data on vibrational relaxation times and dissociation rates. The calculations show that freezing in the nozzle causes the relaxation behind a normal shock wave to be generally different from that in free flight. In a shock tunnel with a nozzle length of 5 meters operating at a reflected-shock pressure of 1000 atmosphere, standard, free-flight conditions are simulated fairly closely in its test section.

Nomenclature

A	=	nozzle cross-sectional area
a_i	=	coefficients in Eq. (1)
C	=	average molecular speed, cm/s
c	=	continuum (free) state
E_v	=	energy level of state v, cm^{-1}, or erg
H	=	enthalpy, erg/g or MJ/kg
I	=	radiation intensity, arbitrary units
$K(v, v')$	=	rate coefficient for v-to-v' transition, cm^3/s
k	=	Boltzmann constant 1.3806×10^{-16} erg/K
M	=	colliding species
m	=	mass of one atom or molecule, g
n	=	number density, cm^{-3}
p	=	pressure, dyne/cm^2 or atm
T	=	translational–rotational temperature, K
T_{ve}	=	hypothetical vibrational temperature of a harmonic oscillator having the same vibrational energy as the given vibrational distribution
T_{v1}	=	vibrational temperature by ratio of $v = 1$ to $v = 0$ state populations
u	=	flow velocity, cm/s
u_s	=	shock velocity in a shock tube, cm/s
v	=	vibrational quantum number, or initial state
v_{max}	=	maximum vibrational quantum number
v'	=	final state vibrational quantum number
(X)	=	mol fraction of species X
x	=	distance from throat or shock wave, cm
σ	=	cross section, cm^2
τ_v	=	vibrational relaxation time, s

Subscripts

m	=	molecule
p	=	peak in radiation
0	=	settling chamber
*	=	nozzle throat

Presented as Paper 0585 at the 44th Aerospace Sciences Meeting and Exhibit, Reno, NV, 9–12 January 2006; received 24 January 2006; revision received 20 March 2006; accepted for publication 21 March 2006.

*Professor, Department of Aerospace Engineering, 373-1 Guseong-dong, Yuseong-gu, Daejeon 305-701, Republic of Korea; cpark216@kaist.ac.kr. Fellow AIAA.

Introduction

In recent years, considerable advancement was made in the technique of testing in a shock tunnel. In a nitrogen stream where high temperature chemical effects are weak, experimental results are found to agree closely with the computational fluid-dynamics calculations (see, e.g., [1,2]). However, in an air stream where chemical reactions are significant, agreement between the calculations and the experimental data are not as close [1,2]. It is not clear whether the observed discrepancy between the experiment and calculation is due to the real gas effect occurring in the flow around the model or due to the well-known thermochemical freezing occurring in the nozzle. That is, one is not sure at this time as to how good a shock tunnel is in simulating the nonequilibrium real gas effects around a vehicle.

The nozzle freezing phenomena have hitherto been calculated using a multitemperature model. But the multitemperature method brings several uncertainties. The first uncertainty is on the accuracy of the multitemperature representation of chemical reaction rates. Second, the extent of the overpopulation of high vibrational states due to vibration–vibration coupling, observed for CO [3] and predicted for N_2 [4,5], and its influence on the flow around a model, are not known. Third, uncertainty concerns the influence of the state-specific reactions in the Zeldovich processes [6,7].

It is the purpose of the present work to answer the question as to how good a shock tunnel is in simulating the nonequilibrium real gas effects. Nonequilibrium real gas effects produce relaxation of several physical quantities in a flow behind a shock wave. Of these, the most important is the variation in density. Density variation causes variation in shock layer thickness, which in turn causes variation in shock shape and, consequently, variation in pressure distribution. If 1) the density ratio across the shock wave, and 2) the relaxation distance of density value behind a shock wave in a shock tunnel test are the same as those in flight, the shock tunnel test can be said to correctly simulate the nonequilibrium real gas effects.

To determine these two characteristic quantities theoretically, a computer code is developed here which calculates the flow conditions using a state-to-state, i.e., master equation, method. State-to-state transition rate coefficients are derived from the forced harmonic oscillator (FHO) model of Adamovich et al. [8]. The calculated FHO rate coefficients are multiplied by a correction factor to numerically reproduce the existing experimental data on vibrational relaxation times and dissociation rates. Calculation is made for the nozzle and behind the normal shock formed in the test section. The calculated postshock flow properties are compared to similar calculations for free-flight conditions to assess the fidelity of the shock tunnel test.

The calculation is focused on two typical shock tunnel dimensions, one with a nozzle of 1 m length operating at a

reflected-shock pressure of 100 atm and the other with a 5 m nozzle operating at 1000 atm reflected-shock pressure. The latter represents the typical operation condition of existing large shock tunnels. If such a shock tunnel cannot simulate the real gas effects, the community must look for a different way of simulating a hypervelocity flow, such as the radiatively heated wind tunnel [9].

The accuracy of the present model is verified first by comparing the location of the calculated peak point of radiation of the N_2 first positive system with the experimental data obtained in a shock tube [10]. Comparison is made also for the vibrational temperature measurement of Hurle et al. [4] and Sharma et al. [11] in a shock tunnel.

The calculations using the computer code so developed, named airtnl.f, generates information on many aspects of the flow, in addition to the answer to the question posed. It predicts nearly the same thermodynamic states in the test section as a traditional two-temperature model. However, behind the normal shock wave, the state-to-state calculation tends to predict an equilibration rate different from the two-temperature method. Overpopulation of the upper vibrational states in the nozzle due to vibration–vibration coupling is made less prominent in air by the strong interaction between N_2 and O. The nozzle freezing phenomenon can, in general, significantly affect the equilibration rate behind the normal shock wave. Hydrogen atoms originating from water vapor can explain the observed acceleration of vibrational relaxation in a shock tunnel.

In the end, the calculations show that the density ratio across the normal shock wave and the density relaxation distance, characterized by the density variation midpoint, in a shock tunnel test are nearly the same as those in free flight if the nozzle length is 5 m and reflected-shock pressure is 1000 atm.

Chemistry

Chemical Model

Air is considered to consist of 76.6% N_2 and 23.4% O_2 by mass, plus a small concentration of H, forming a mixture of N, O, N_2, O_2, NO, and H at high temperatures. H-atoms exist in a small concentration as an impurity in shock tunnel flows because of the water vapor in the driven tube: water molecules adsorb on the driven tube wall while the driven tube is opened for cleaning. In the reflected-shock region, water molecules dissociate into H- and O-atoms. In the nozzle, H-atoms most likely remain as H-atoms because their three-body recombination rates will be small due to their low concentrations. Even though their concentration is small, the H-atoms can affect vibrational relaxation because of their high efficiency [12,13]. In comparison, other heavy impurity species such as Fe are much less effective in causing vibrational transitions [14]. The H-atoms are excluded in calculating mass, momentum, or energy of the flow because of their low concentrations.

The three molecules, N_2, O_2, and NO, are considered to have only the ground electronic state. A two-term Dunham expansion is used in calculating vibrational energy levels of these molecules. One level above the maximum vibrational quantum number $v_{\max}$ is considered to be the dissociation limit. This results in $v_{\max}$ values of 47, 37, and 39 for N_2, O_2, and NO, respectively. Dissociation energy is calculated to be 78567.1, 41616.1, and 52275.6 cm^{-1}, respectively, as compared with the true values of 78740, 41280, and 52335 cm^{-1}.

Table 1 Comparison of equilibrium thermodynamic states between present model and JANAF model [15] at 1 atm

	$H = 10$ MJ/kg		$H = 20$ MJ/kg	
	Present	JANAF	Present	JANAF
T, K	4883	4991	6540	6541
N mol fraction	2.025e − 2	2.561e − 2	3.286e − 2	3.307e − 2
O mol fraction	3.228e − 1	3.235e − 1	2.861e − 1	2.854e − 1
N_2 mol fraction	6.346e − 1	6.298e − 1	3.806e − 1	3.785e − 1
O_2 mol fraction	2.766e − 3	2.213e − 3	8.056e − 5	9.005e − 5
NO mol fraction	1.959e − 2	1.881e − 2	4.653e − 3	4.784e − 3
NO^+ mol fraction	0.000e − 0	2.729e − 5	0.000e − 0	2.248e − 4

Rotational temperature is assumed to be the same as the translational temperature. The thermodynamic state variables calculated by this model are compared with those determined from the JANNAF thermochemical data base [15] in Table 1. The errors produced by the present model are small, and therefore are neglected.

To verify the accuracy of the present method, calculations have been made for the experiments run with N_2 [4,11] and CO [3]. N_2 flows were treated as an N_2–O_2 mixture flow with an N-to-O elemental mass ratio of 10^5. For the CO flow, a separate code was written in which energy levels are modeled in a similar manner.

State-to-State Transition Rate Coefficients

As mentioned, the reference values of vibrational state-to-state transition rate coefficients are determined through the use of the FHO model developed by Adamovich et al. [8]. Three types of reference rate coefficients are calculated by the FHO model: vibration-to-translation (V–T), vibration-to-vibration (V–V) within the same species, and vibration-to-vibration energy transfers between different species. The reference values of bound-free transition rates are obtained by first continuing the Dunham expansion to levels beyond $v_{\max}$ (by 20 levels), carrying out the V–T transition calculations, and summing over the final states.

The FHO method requires iterations of varying degrees [8]. Accuracy of the calculated values depends partly on the degree of iterations used. But, high degree of iterations needed for high accuracy was seen to produce divergence of the calculation. To ensure convergence, a low level of iteration was used in the present work.

One can write a transition rate coefficient in general in the form

$$K = \sigma C \exp(-\Delta E/kT)\ \text{cm}^3/\text{s} \tag{1}$$

Here $C = \sqrt{8kT/(\pi\mu)}$, where μ is the reduced mass $\mu = m_m m_M/(m_m + m_M)$, and ΔE is the threshold energy $\Delta E = E_{v'} - E_v$.

For the transitions among high v, collisions are classical. Therefore, the σ should be a fraction of the elastic cross sections which are typically 1.5×10^{-15} cm^2. The largest σ for the bound-bound transitions occurs for the $v_{\max-1}$-to-$v_{\max}$ transition. According to the FHO calculation, this largest σ is in the range from 1.5×10^{-16} to 6×10^{-16} cm^2 for N_2, O_2, and NO. Therefore, the FHO cross section values are considered reasonable for the transitions among the highly excited states.

In calculating K for the bound-free transitions, the σ value for the $v_{\max}$ state is first calculated as described. For the levels below $v_{\max}$, K is seen to decrease roughly as $1/(v_{\max} + 1 - v)$ among the high v. To produce a smoothly varying reference K, the reference K values for the bound-free transitions are expressed as

$$K = \sigma C \exp(-\Delta E/kT)/(v_{\max} + 1 - v)\ \text{cm}^3/\text{s} \tag{2}$$

These FHO rate coefficients are evaluated at five temperatures, 400, 1200, 3600, 10,800, and 32,400 K. The calculated values are fitted by a five parameter expression

$$K = \exp(a_1/z + a_2 + a_3 \ell_n z + a_4 z + a_5 z^2) \tag{3}$$

where $z = 1000/T$.

Because the σ values for the high v states are reasonable, they are used without correction. However, for the transitions among low levels, for which quantum effects are large, the FHO rate coefficients for the V–T transitions must be consistent with the known vibrational relaxation time data. Therefore, for the V–T transitions, the FHO rate coefficients are multiplied by a linearly varying correction factor in the form

$$K \text{ used} = \text{FHO } K \times \text{ correction factor} \tag{4}$$

where

Table 2 Correction factors to state-to-state transition rate coefficients for $v = 0$

Species	M	Correction factor	Source of experiment
N_2	N	$3.36(4500/T)^{0.85}$	Millikan and White [16]
	O	$3.24(4500/T)^{3.7}$	Eckstrom [17]
	N_2	$0.302(T/4500)^{0.50}$	Millikan and White [16]
	O_2	$0.302(T/4500)^{0.50}$	as for N_2–N_2
	NO	$0.618(4500/T)^{0.17}$	Millikan and White
	H	1	no experimental data
O_2	N	$0.248(4500/T)^{0.54}$	Eckstrom (N_2–O) [17]
	O	$12.6(4500/T)^{2.05}$	Kiefer and Lutz [18]
	N_2	$0.657(4500/T)^{0.50}$	Millikan and White [16]
	O_2	$0.557(4500/T)^{0.20}$	Millikan and White
	NO	$0.712(4500/T)^{0.55}$	Millikan and White
	H	1	no experimental data
NO	N	$12.6(4500/T)^{2.05}$	Kiefer and Lutz (O_2–O) [18]
	O	$12.6(4500/T)^{2.05}$	Kiefer and Lutz (O_2–O)
	N_2	$30(4500/T)^{3.2}$	Wray (NO–O) [19]
	O_2	$30(4500/T)^{3.2}$	Wray (NO–NO)
	NO	$30(4500/T)^{3.2}$	Wray
	H	1	no experimental data
CO	CO	$0.103(T/4500)^{0.23}$	Millikan and White [16]
	Ar	$0.195(4500/T)^{0.14}$	Millikan and White

$$\text{Correction factor} = (\text{correction factor for } v = 0) \times \frac{v_{\max} - v}{v_{\max}} + \frac{v}{v_{\max}} \tag{5}$$

The correction factor for $v = 0$ is determined by comparing with the known vibrational relaxation time data as described next.

Correction Factors for Vibration-to-Translation Energy Transfer

It is known that the V–T transition rate coefficients between the neighboring states among the lowest few vibrational levels behave almost as a harmonic oscillator. It is well known that, for the harmonic oscillator, the vibrational relaxation time is related to the $v = 1$ to $v = 0$ transition rate coefficient $K(1, 0)$ by

$$\tau_v = n_M K(1, 0)[1 - \exp(-E_1/kT)] \tag{6}$$

The corrective multiplication factor for $v = 0$ in Eq. (5) is chosen so that the theoretical τ_v value agrees with the measured value [16–19]. The sources of the experimental data and the correction factors for $v = 0$, calculated by the forced harmonic oscillator model for the V–T energy transfer, are summarized in Table 2. The vibrational relaxation times resulting from the transition rate values so corrected are compared with the experimental data in Figs. 1a–1c. Fairly good agreement is seen.

Vibration-to-Vibration Energy Transfer

The calculated V–V transition rate coefficients are compared with the experimental data for the N_2–NO mixture [20]. The experimental data are given in the form of transition probability, which is the ratio of transition rate to elastic collision rate. The elastic collision rate was calculated in [20] using the $\Omega^{(2,2)}$ values for the Lennard–Jones potential given in [21]. The same procedure was followed here in deducing rate coefficient values from the transition probability values. For the N_2–NO collisions, this led to a multiplicative correction factor of $2.5(T/1000)^{0.21}$. The resulting transition probability values are compared with the measured values in Fig. 2. This correction factor was applied to all V–V transitions, i.e., between the different species, among the same species, and to all v and v'.

For comparison purposes, a similar test was made for the CO–N_2 coupling. The FHO rate coefficients reproduced the experimental data [22] without any correction. For the CO–CO V–V coupling, the rate coefficient is tested by comparing the calculated vibrational population distribution with the experimental data of [3]. A factor of 45 was needed to reproduce the experimental data.

Bound-Free Transitions

The bound-free transition rate coefficients control mainly the dissociation and recombination rates; these rates are proportional to the transition rate coefficients. The multiplicative correction factors for the bound-free transitions for N_2 and O_2 are determined by comparing with the existing dissociation rate coefficients [23–25]. In calculating the dissociation rate coefficients from the given transition rate coefficients, the quasi-steady state calculation described on page 95 of [26] was followed. For NO, dissociation rate coefficients are not known well. Therefore, the correction factor was determined as a logarithmic average between those for N_2 and O_2. In Table 3, the correction factors, calculated by the FHO model for bound-free transitions, and the sources for comparison are summarized. The dissociation rate coefficients of N_2 and O_2 so calculated are compared with experimental data in Fig. 3.

Collisions with H

For the collisions of N_2, O_2, and NO with H-atoms, there are no vibrational relaxation time data to compare. Vibrational relaxation times have been measured in a shock tube for N_2–H_2O mixtures [12,13]. Even though H_2O is sure to dissociate and produce H-atoms eventually, H-atoms are not present in the early part of a postshock flow. Therefore, the shock tube experiment cannot be considered to be a test of the effect of H-atoms. Therefore, the FHO values are used directly for the V–T transitions.

The σ for the bound-free K of N_2, O_2, and NO with collisions with H-atoms, for the $v_{\max}$ state, are calculated (by summing up the bound–bound transitions to the hypothetical levels above $v_{\max}$) to be about 8×10^{-15} cm^2 for the N_2–H collisions, 6×10^{-15} cm^2 for the O_2–H collisions, and 4×10^{-15} cm^2 for the NO–H collisions. These σ values are of the order of the elastic cross sections, which are considered reasonable. Therefore, these values are used also without correction.

State-to-State Zeldovich Reaction Rates

The state-specific reaction rate coefficients for the two Zeldovich reactions $N_2 + O \rightarrow NO + N$ and $NO + O \rightarrow O_2 + N$ have been calculated by Bose and Candler [6,7]. These rate coefficients are used in the present work.

Calculation Procedures

Master Equation

The system of ordinary differential equations of the type

$$u\frac{dn_v}{dx} = \Sigma_{v'} K(v', v) n_{v'} n_M - \Sigma_{v'} K(v, v') n_v n_M + K(c, v) n_A n_B n_M - K(v, c) n_v n_M \tag{7}$$

was written accounting for

1) the V–T processes for all v values and v' values of up to $v \pm 5$;

2) the V–V processes in which the colliding particle is a molecule of the same species: for all v and up to $v' = v \pm 2$ (transitions of the colliding particles are considered to occur within the range of v and $v' = 0$ to 2);

3) the V–V processes between different species; between N_2 and NO, up to $N_2(v = 10)$ and $NO(v = 4)$; between NO and O_2, up to $O_2(v = 4)$ and $NO(v = 10)$;

4) the bound-free transitions for all v values.

5) the Zeldovich reactions for v and v' values of up to 15.

The concentrations of N_2, O_2, and NO are calculated by summing up the number densities over all v values. The concentration of N and O are deduced from those of N_2, O_2, and NO through the use of the elemental and total mass conservation laws.

Flow Field

The flow process was assumed to be one-dimensional and inviscid. For most of the calculations, area ratio of the nozzle was described by a hyperbolic shape

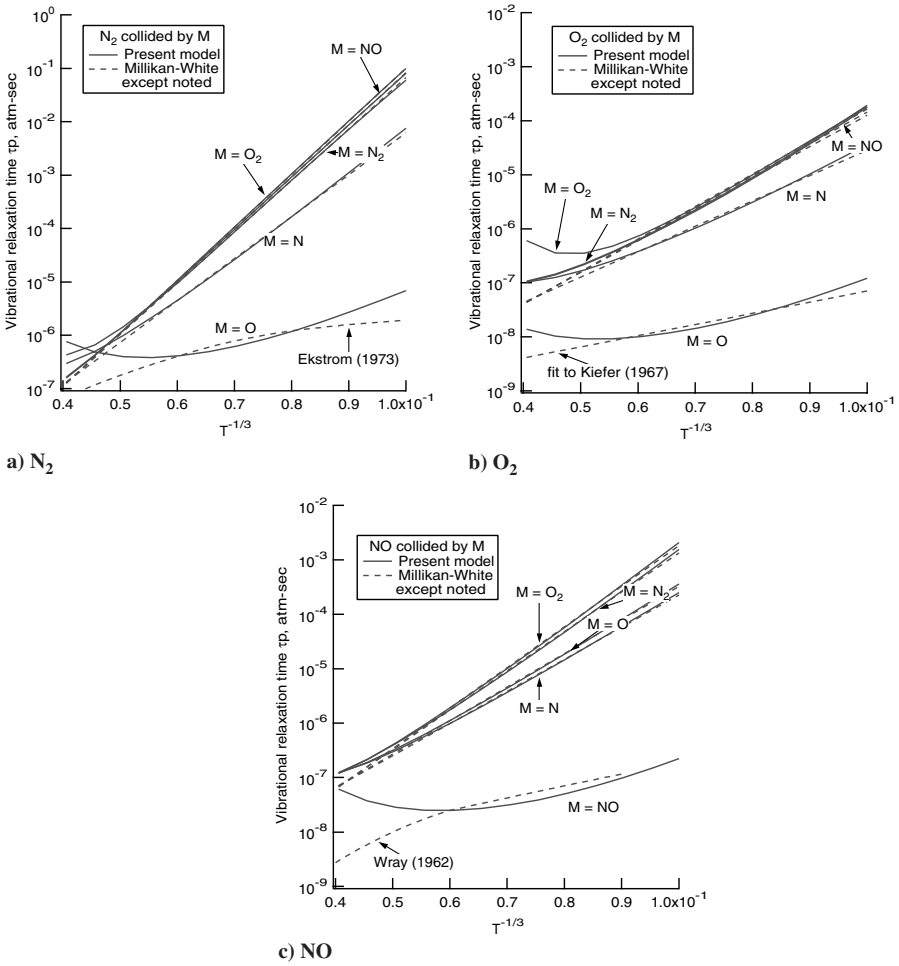

Fig. 1 Comparison of τ_v derived by the present procedure with the experimental data.

$$\frac{A}{A^*} = 1 + Bx^2 \tag{8}$$

Most of the calculations were performed for the exit area ratio of 1000. For the calculations for the experiments by Bender [3], Hurle et al. [4], and Sharma et al. [11], the area ratios determined in the experiments were used.

The flow was first assumed to be in equilibrium to a point slightly downstream of the nozzle throat. Nonequilibrium calculation was started at that point. At the test section, a normal shock wave of zero thickness was assumed. The postshock condition was calculated using the Rankine–Hugoniot relation for a frozen flow. Nonequilibrium calculation was made from that point on.

For comparison purposes, hypothetical free-flight conditions producing the same pitot impact pressure, ρu^2, and enthalpy, $0.5u^2$, were calculated also. The freestream temperature was assumed to be 300 K. The vibrational distributions for N_2 and O_2 (no NO) were taken to be Boltzmann at 300 K.

Characteristic Quantities

For the three molecular species N_2, O_2, and NO, two different vibrational temperatures were defined. First is the temperature defined by the ratio of the number density of the $v = 1$ state to that of

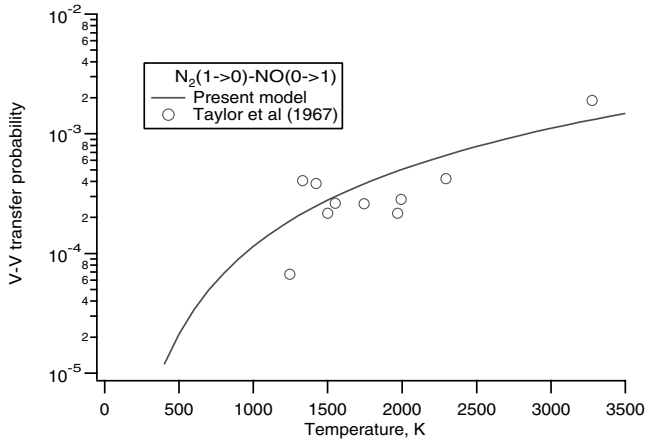

Fig. 2 Comparison of vibrational energy coupling probability between N_2 and NO, present model and experiment in [19].

Table 3 Correction factors to the bound-free transition rate coefficients

Species	M	Correction factor	Source of experiment
N_2	N	$43(4500/T)^{3.0}$	$4.3 \times N_2$–N_2 [23,25]
	O	$43(4500/T)^{3.0}$	$4.3 \times N_2$–N_2 [23,25]
	N_2	$10(4500/T)^{3.0}$	Baulch et al. [23]
	O_2	$10(4500/T)^{3.0}$	Baulch et al. (N_2–N_2)
	NO	$10(4500/T)^{3.0}$	Baulch et al. (N_2–N_2)
O_2	N	$12.5(4500/T)^{3.0}$	Baulch et al. (O_2–O) [24]
	O	$12.5(4500/T)^{3.0}$	Baulch et al.
	N_2	$2.5(4500/T)^{3.0}$	Baulch et al. (O_2–O_2)
	O_2	$2.5(4500/T)^{3.0}$	Baulch et al.
	NO	$2.5(4500/T)^{3.0}$	Baulch et al. (O_2–O_2)
NO	N	$23(4500/T)^{2.05}$	log avg of N_2 and O_2
	O	$23(4500/T)^{2.05}$	log avg of N_2 and O_2
	N_2	$5.0(4500/T)^{3.2}$	log avg of N_2 and O_2
	O_2	$5.0(4500/T)^{3.2}$	log avg of N_2 and O_2
	NO	$5.0(4500/T)^{3.2}$	log avg of N_2 and O_2

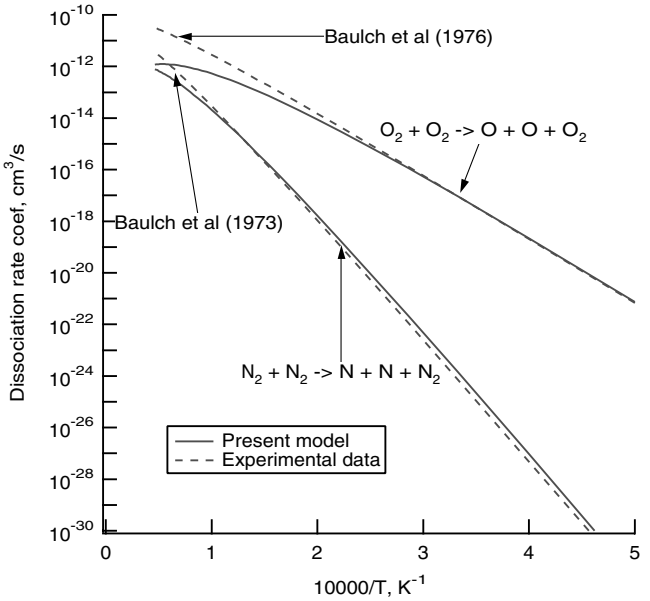

Fig. 3 Comparison of dissociation rate coefficient between present model and experimental data in [23].

the $v = 0$ state, which is termed here zero-slope vibrational temperature and designated by T_{v1}. The second is the hypothetical Boltzmann vibrational temperature of a harmonic oscillator having the same vibrational energy as the vibrational distribution under consideration, which is termed energy-equivalent vibrational temperature and designated by T_{ve}.

In characterizing the equilibration distance behind a normal shock wave, two characteristic quantities are defined. The first is the midpoint of variation in density. This point is important because density affects pressure distribution, as mentioned in the Introduction. The second is the peak-radiation point. In N_2 and air, radiation in the wavelength region from about 500 to about 700 nm produced by the first positive (1+) band system of the N_2 molecule is most prominent. In [10], the peak point in the intensity of this radiation and the point where this radiation asymptotes to the equilibrium value have been measured. Of these two characteristic points, the peak point is more clearly definable. The energy level of the emitting state of the N_2 1+ radiation, $B^3\Pi_g$, is 59307 cm^{-1}. Its excitation temperature can be taken to be T_{v1} because of the well-known strong coupling between the electronic mode and the vibrational mode for N_2. Therefore, the intensity of the N_2 1+ system can be approximated by

$$I = \text{ a constant} \times n_{N_2} \exp(-1.4388 \times 59307/T_{v1}) \qquad (9)$$

In [10], the time to the peak of this radiation τ was measured in a shock tube experiment. This τ is the distance to the peak point from the shock front x_p, shown in Fig. 4 [27], divided by the shock speed. In [10], this τ was then multiplied by the preshock (freestream) pressure to obtain the so-called $p\tau$ parameter

$$p\tau = (x_p/u_s) \times \text{ freestream pressure} \qquad (10)$$

This quantity was calculated in the present work for the purpose of comparison with the experimental data.

Numerical Method

An implicit integration subroutine accurate to the third order along the diagonal and second order over the off-diagonal elements was used to integrate the resulting system of 127 ordinary differential equations. The code was written in FORTRAN 77, and was run on an IBM PC, using Windows XP, with a Pentium 4 CPU, using the FORTRAN compiler, Visual FORTRAN. The source code is 3497 lines long and needs two input files: unit 7 containing the coefficients a_i in Eq. (1), which is 4572 lines long, and unit 5 containing a short list of run parameters. Typically, nozzle flow calculation is completed within 1.5 h, and the two postshock flow calculations, one for the flow in test section and the other for free flight, require about 3 h.

Results

Validation of Method

Postshock Equilibration Time

Accuracy of the present method was tested first by comparing the peak-radiation point time constant $p\tau$ defined in Eq. (10) for an undisturbed freestream flow at 300 K, i.e., flight conditions, with the shock tube data [10]. The concentration of the H-atoms was varied; there were no significant differences in the results. The comparison is given in Fig. 5. As seen here, the present method correctly reproduces the peak-radiation point. The two-temperature model reproduces the experimental data also, as expected.

Line-Reversal Measurement of Hurle et al. [4]

In [4], vibrational temperature was measured in a shock tunnel using the line-reversal method. In that experiment, presence of water vapor is suspected. Therefore, the concentration of the H-atoms was varied arbitrarily until the calculation reproduced the measured values. The nozzle area ratio distribution is that given by the measured static pressure values.

In Fig. 6, the result is shown. As seen here, the experimental data can be reproduced when the H-atom concentration is assumed to be 680 ppm, which corresponds to H_2O concentration of 340 ppm. This concentration of H_2O is plausible. In comparison, if H-concentration is zero, the calculated vibrational temperatures are significantly higher than the measured values.

Raman Measurement of Sharma et al. [11]

In [11], vibrational distribution of N_2 was measured in a shock tunnel using the spontaneous Raman spectroscopy. Precaution was taken in that experiment to minimize water vapor and, therefore, hydrogen concentration was assumed to be zero in numerical reconstruction of the case. The result of the calculation is compared with the experimental data in Fig. 7. As seen here, the present model reproduces the measured data within the accuracy of the measurement.

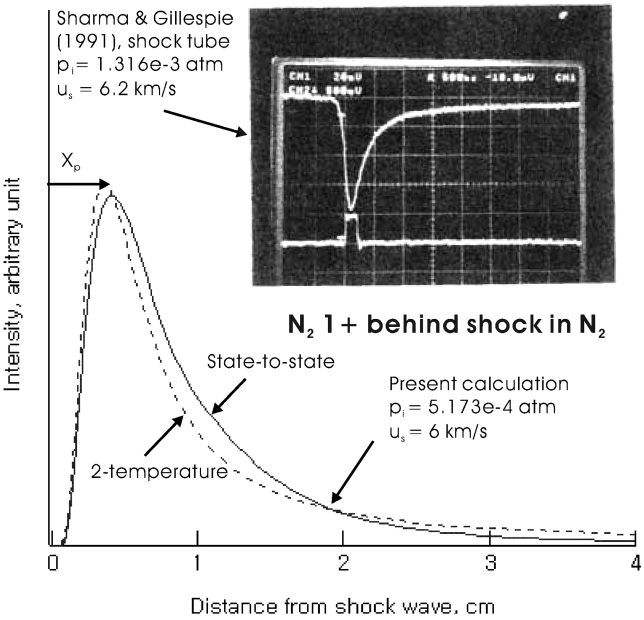

Fig. 4 Variation of N_2 first positive radiation: comparison between present calculation and typical experimental data [27].

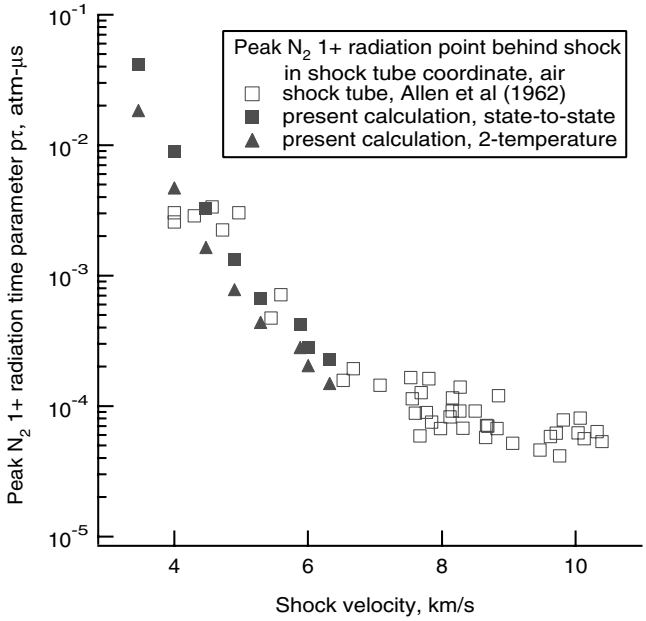

Fig. 5 Characteristic time parameter for peak in radiation of N_2 first positive system.

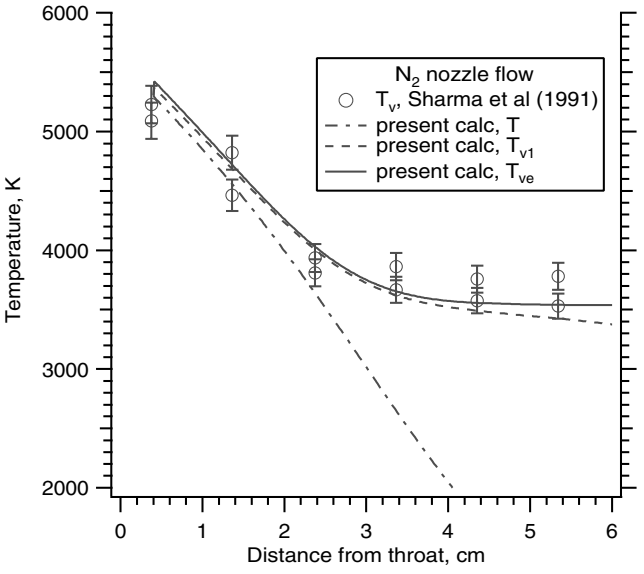

Fig. 7 Comparison of vibrational temperature for the experiment [11].

Nozzle Flows

Freezing Behavior

The general behavior of the solutions is shown for the case of $p_0 = 100$ atm and $H = 10$ MJ/kg in Figs. 8a and 8b. As seen from Fig. 8a, there is little difference between the zero-slope vibrational temperature T_{v0} and the energy-equivalent temperature T_{ve}. Freezing behavior appears both in vibrational temperatures and in species mol fractions.

At around $x = 30$ cm ($A/A_* \approx 100$), concentration of N-atoms disappears (numerical values become slightly negative) and vibrational temperatures of NO rise. This phenomenon could be interpreted as follows: in the beginning, the first Zeldovich reaction $N_2 + O \rightarrow NO + N$ occurs in the reverse direction, and thus the N-atoms are removed. Simultaneously, the N_2-to-NO vibration–vibration coupling raises the vibrational temperature of NO (the downward transitions of N_2 cause upward transitions of NO). The vibrationally excited NO molecules can then produce N-atoms via the second Zeldovich reaction $NO + O \rightarrow O_2 + N$, in a process which cools the vibrational temperature of NO. The vibrational heating of NO predicted here should not be a surprise because similar behaviors are exploited commonly to produce a gasdynamic laser.

In Fig. 9, the atom mass fractions (sum of N and O masses divided by the total mass) at the nozzle exit are shown for a nozzle of 20, 100,

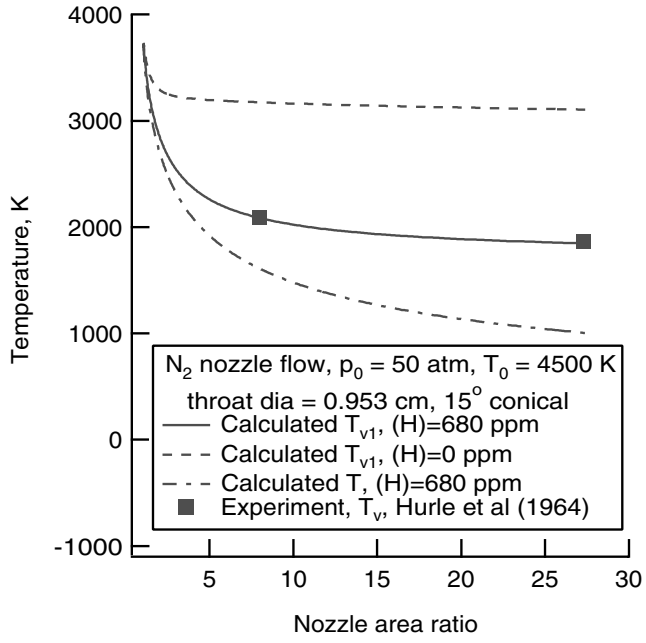

Fig. 6 Comparison of vibrational temperature for the experiment [6].

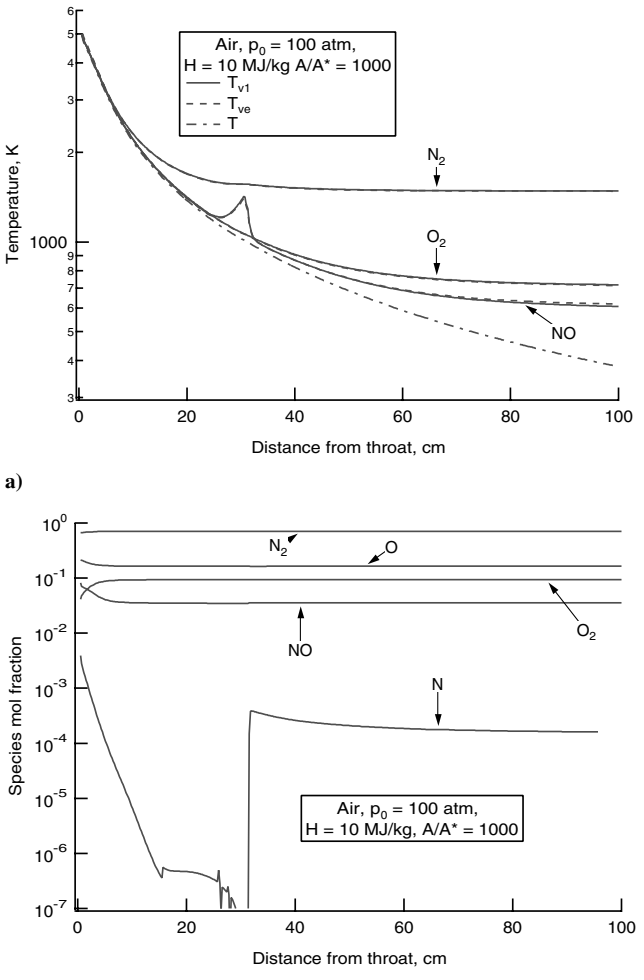

Fig. 8 Typical behavior of the nozzle flow in air: $p_0 = 100$ atm, $H = 10$ MJ/kg, $A/A_* = 1000$.

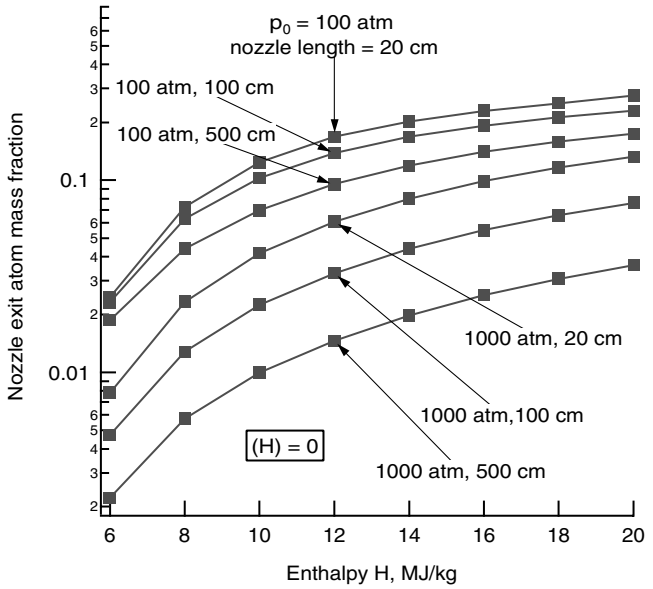

Fig. 9 Atom mass fraction at nozzle exit.

and 500 cm lengths at p_0 of 100 and 1000 atm. As the figure shows, atom mass fractions are significant even for p_0 of 1000 atm and nozzle length of 500 cm.

Population Distribution

The population distribution at the nozzle exit for the conditions of Figs. 8a and 8b is shown in Fig. 10 by the solid curve. There is a sharp bend in the distribution at the energy level of about 22, 000 cm^{-1}, which corresponds to $v \approx 11$ and also to the threshold energy of the first Zeldovich reaction; the reverse reaction of the first Zeldovich reaction tends to produce N_2 in vibrational states above this level. If the N_2–O collisions are removed in the calculation, the distribution changes to that shown by the dashed curve. The N_2–O collisions are very efficient in vibrational relaxation [17]. Notice the population inversion at high levels.

To understand the reason for the strange population distribution for air, calculation was made for an N_2 flow with the same p_0 and T_0. The results are presented in Fig. 10 and Table 4, using $p_0 = 100$ atm, H = 10 MJ/kg, and $A/A_* = 1000$ ($T_0 = 5678$ K) for air, and H = 7.4 MJ/kg ($T_0 = 5672$ K) for N_2. As seen therein, population distribution for N_2 is very different from that of air. Thus, the strange population distribution for air is attributable to air chemistry, i.e., fast

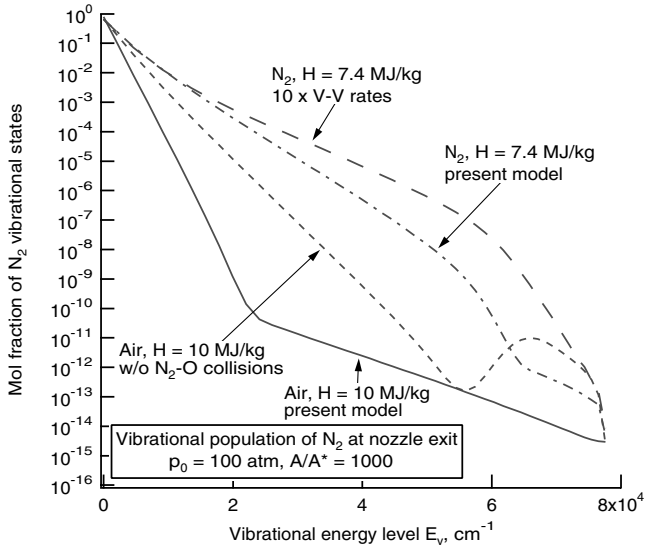

Fig. 10 Population distribution at nozzle exit for air and N_2, $T_0 \approx 5675$ K.

Table 4 Nozzle exit vibrational temperatures of N_2 in air and N_2

Model	T_{v1}	T_{ve}
Air, present model	1483	1481
Air, N_2–N_2 V–V rate = 0	1523	1508
Air, N_2–N_2 V–V rate × 10	1510	1509
Air, without N_2–O interactions	2392	2450
N_2, present model	3063	3326
N_2, N_2–N_2 V–V rate × 10	2884	3310

N_2–O V–T energy transfer, fast N_2–NO V–V energy transfer, and state-specific Zeldovich reactions.

In Fig. 10, the N_2 distribution predicted by the present model shows a weaker overpopulation of upper states, i.e., Treanor distribution, than predicted in [4,5]. Only when the V–V rates are multiplied by a factor of 10, does the Treanor distribution become significant. The smooth variation in the high levels for this case is similar to that assumed in [5].

Comparison with One- and Two-Temperature Models

In Figs. 11a and 11b, the present state-to-state results are compared with a one-temperature calculation and a Landau–Teller

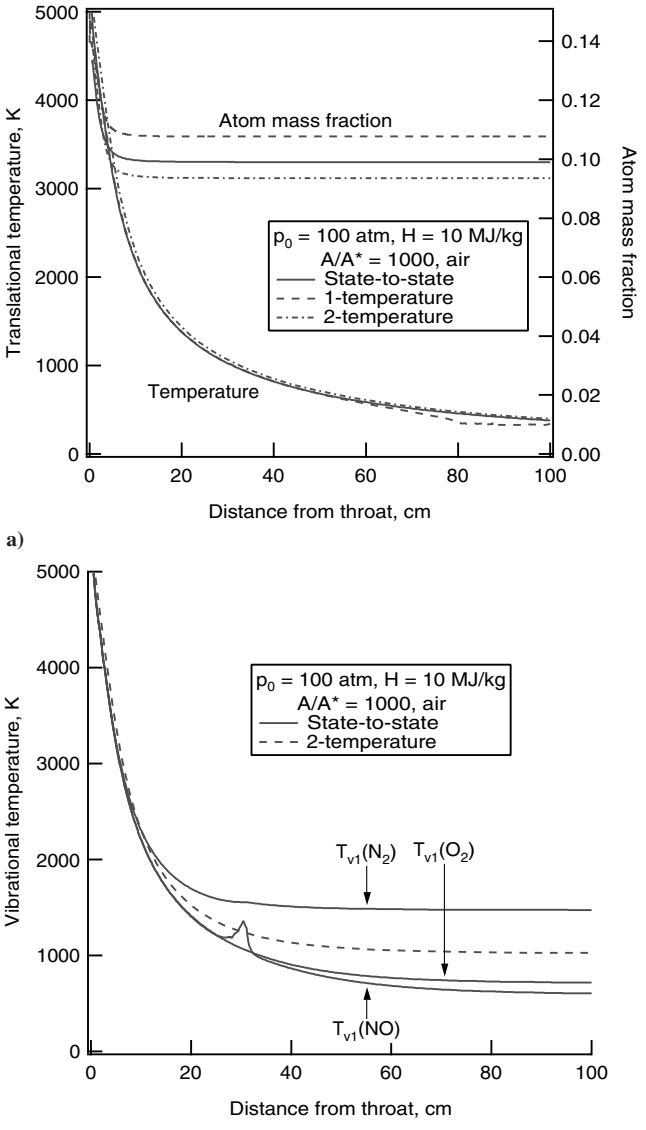

Fig. 11 Comparison between present calculation with the one- and two-temperature calculations.

type two-temperature calculation. The rate coefficients in the one-temperature and two-temperature calculations are the same as those used implicitly in the state-to-state calculations. As these figures show, the state-to-state calculation and the one/two-temperature calculations yield nearly the same flow conditions in the nozzle exit. The vibrational temperature in the two-temperature model seems to be an approximate mean value of the three vibrational temperatures in the state-to-state solution.

Post-Shock Flows

Test Section Flow vs Free-Flight Flow

In Fig. 12a, the temperatures and the N_2 1+ radiation behind a normal shock wave formed in the test section are shown for a typical case. In Fig. 12b, a similar result is shown for a free-flight case in which $0.5u^2$ and ρu^2 are the same as those in Fig. 12a. As seen in these figures, the test section flow equilibrates faster than in free flight. This difference in the equilibration time is due mostly to the dissociation present in the shock tunnel test section stream. The existence of the high population of the upper vibrational states accounts for approximately 5% of the difference.

In Fig. 13, the variations in atom mass fraction and density are compared between the test section flow and the free-flight flow. That

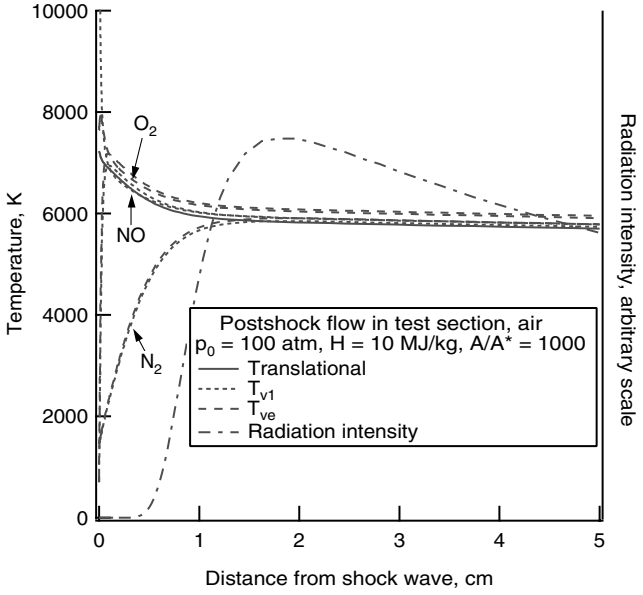

a)

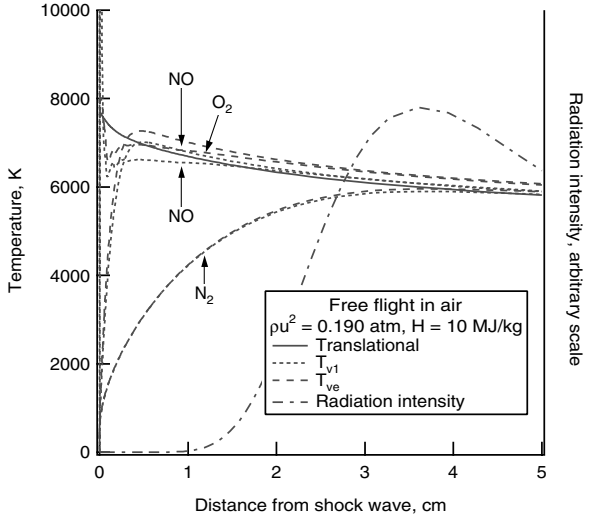

b)

Fig. 12 Variation in temperature and N_2 first positive radiation behind a normal shock wave.

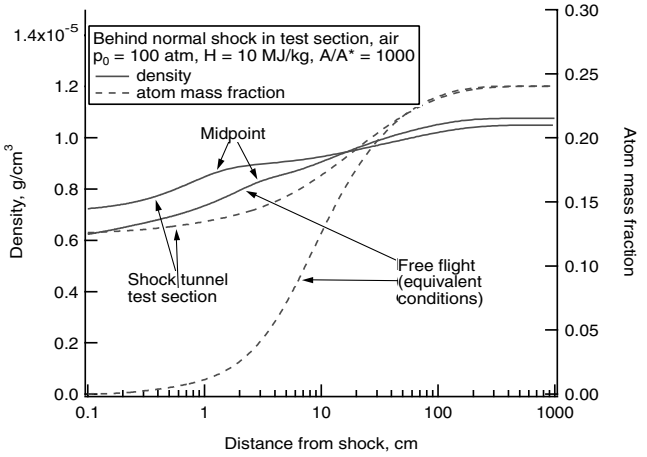

Fig. 13 Comparison of density and atom mass fraction behind a normal shock wave.

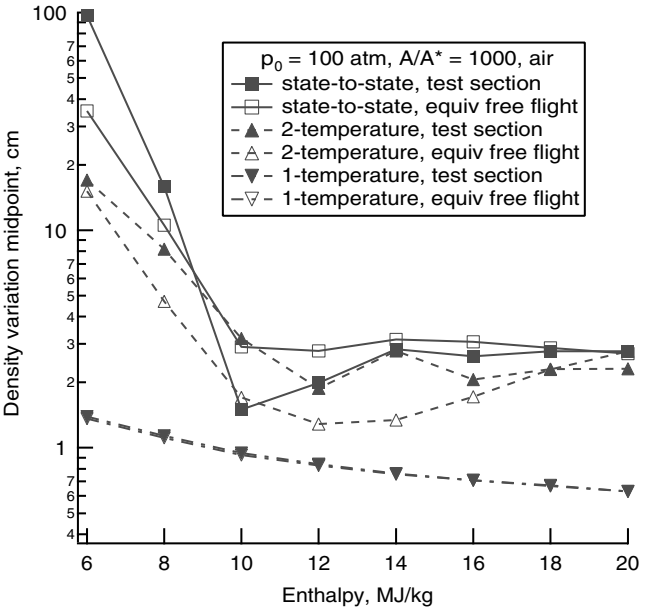

Fig. 14 Comparison of density variation midpoint calculations behind a normal shock wave.

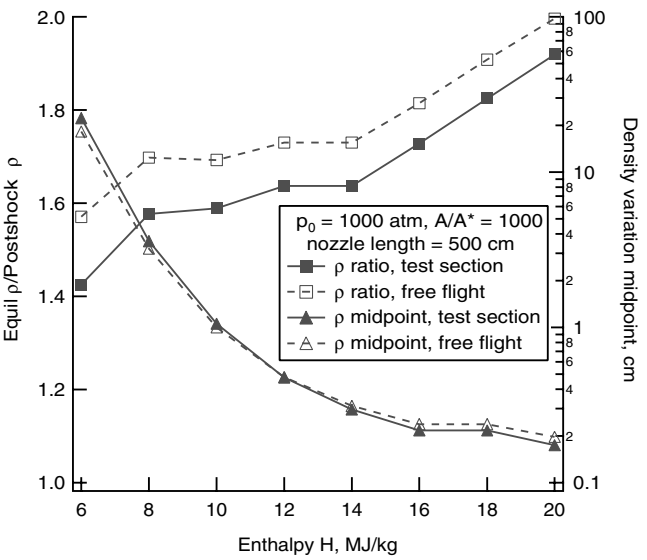

Fig. 15 Ratio of density at equilibrium to behind shock wave and variation midpoint distance.

Table 5 Flow properties for $p_0 = 1000$ atm, nozzle length = 500 cm, $A/A_* = 1000$

Enthalpy, MJ/kg	6	8	10	12	14	16	18	20
Settling chamber temp T_0, K	4383	5343	6224	7072	7840	8497	9057	9545
Nozzle exit								
Pressure, atm	5.266e − 2	2.920e − 2	2.161e − 2	1.730e − 2	1.367e − 2	1.227e − 2	1.116e − 2	1.022e − 2
Density, g/cm^3	1.897e − 5	1.386e − 5	1.117e − 5	9.342e − 6	7.995e − 6	7.045e − 6	6.321e − 6	5.710e − 6
Velocity, m/s	3081	3740	4243	4683	5088	5449	5789	6110
T, K	974	736	674	643	590	599	604	609
$T_{v1}(N_2)$, K	1340	1073	1068	1079	1050	1083	1102	1122
$T_{ve}(N_2)$, K	1337	1070	1066	1077	1048	1080	1100	1120
$T_{v1}(O_2)$, K	1011	792	735	707	664	671	675	680
$T_{ve}(O_2)$, K	1007	789	732	705	661	668	673	678
T_{v1}(NO), K	993	753	692	663	613	623	630	636
T_{ve}(NO), K	989	750	690	660	611	621	628	634
Atom mass fraction	2.205e − 3	5.684e − 3	9.837e − 3	1.443e − 2	1.959e − 2	2.493e − 2	3.035e − 2	3.576e − 2
N mol fraction	1.16e − 5	1.27e − 8	2.08e − 8	4.10e − 8	8.06e − 8	1.43e − 7	2.30e − 7	3.50e − 7
O mol fraction	3.96e − 3	1.02e − 2	1.76e − 2	2.57e − 2	3.47e − 2	4.39e − 2	5.33e − 2	6.24e − 2
N_2 mol fraction	0.764	0.766	0.764	0.762	0.758	0.755	0.752	0.748
O_2 mol fraction	0.184	0.184	0.181	0.176	0.171	0.166	0.161	0.155
NO mol fraction	4.79e − 2	4.01e − 2	3.74e − 2	3.66e − 2	3.56e − 2	3.51e − 2	3.40e − 2	3.38e − 2
Immediately behind normal shock wave in test section								
Pressure, atm	1.352	1.470	1.531	1.562	1.588	1.606	1.634	1.657
Density, g/cm^3	8.652e − 5	6.930e − 5	5.751e − 5	4.879e − 5	4.245e − 5	3.751e − 5	3.385e − 5	3.576e − 5
T, K	5482	7416	9273	11,050	12,923	14,720	16,510	18,289
Velocity, m/s	621	693	766	834	898	960	1019	1075
Far behind normal shock wave in test section								
Pressure, atm	1.467	1.606	1.671	1.708	1.746	1.775	1.813	1.847
Density, g/cm^3	1.330e − 4	1.185e − 4	9.938e − 5	8.679e − 5	7.958e − 5	7.419e − 5	7.031e − 5	6.690e − 5
T, K	3583	4133	4919	5585	6012	6321	6570	6783
Velocity, m/s	404	405	443	469	479	485	490	496
Atom mass fraction	9.115e − 2	0.1697	0.2220	0.2597	0.3025	0.3488	0.3969	0.4462
Density variation midpoint, cm	24.13	3.698	1.067	0.4771	0.2941	0.2159	0.1830	0.1480
N_2 1+ peak point, cm	0.4449	0.2555	0.1477	0.1025	6.819e − 2	5.908e − 2	4.809e − 2	3.803e − 2

atom mass fraction is very different between the two cases is clearly seen here. There is a bulge, i.e., a negative peak in the second derivative, in the middle of density variation for both cases. This is due to the dissociation of O_2 that occurs before the dissociation of N_2.

In Fig. 14, the density variation midpoint values are compared between the test section flows and free-flight flows for the state-to-state, one-temperature, and two-temperature calculations for $p_0 = 100$ atm. For the state-to-state case, the test section flow equilibrates slower than the free-flight flow at enthalpies below 9 MJ/kg and faster at higher enthalpies. Two-temperature calculations predict uniformly slower equilibration in the test section than in free flight. One-temperature calculations predict the same equilibration rates. Numerically, the state-to-state calculation predicts generally slower equilibration than the two- or one-temperature methods. The one-temperature method predicts the fastest equilibration.

Large Shock Tunnels

In Fig. 15, the ratio of densities between the equilibrium region (large x) and the point immediately behind the shock wave ($x = 0$), and the density variation midpoint distance for the test section flow and the free-flight flow, are shown for $p_0 = 1000$ atm, nozzle length of 500 cm, with no atomic hydrogen. The figure indicates that the density variation midpoint of the flight case is closely reproduced in the test section for this case. The density ratio is slightly different between the test section flow and the free-flight flow. However, the difference is small enough to be tolerated. This means that, for this large facility operating at high reflected-shock pressures, simulation of the free-flight conditions is fairly close. Though not shown, the case of 500 ppm of H-atom concentration shows nearly identical results for this case.

The flow conditions are given in detail in Table 5 for this large facility case for $p_0 = 1000$ atm, for the enthalpy range from 6 to 20 MJ/kg. The free-flight conditions corresponding to those in Table 5 are presented in Table 6. As seen in Table 5, the difference between T_{v1} and T_{ve} is negligible at the nozzle exit for such a large high pressure facility. The degree of simulation is generally good in all aspects.

Discussion

The foregoing results show that a state-to-state description leads to a nozzle freezing phenomenon nearly the same as the two-

Table 6 Flow properties in free-flight conditions corresponding to those in Table 5

Enthalpy, MJ/kg	6	8	10	12	14	16	18	20
Immediately behind normal shock wave in free flight								
Pressure, atm	1.376	1.488	1.546	1.576	1.602	1.620	1.648	1.672
Density, g/cm^3	8.364e − 5	6.783e − 5	5.639e − 5	4.790e − 5	4.173e − 5	3.693e − 5	3.339e − 5	3.048e − 5
T, K	5784	7711	9638	11,565	13,492	15,419	17,346	19,273
Velocity, m/s	572	662	741	812	878	939	997	1051
Far behind normal shock wave in free flight								
Pressure, atm	1.477	1.614	1.679	1.717	1.754	1.782	1.820	1.853
Density, g/cm^3	1.337e − 4	1.189e − 4	9.976e − 5	8.712e − 5	7.989e − 5	7.446	7.054e − 5	6.710e − 5
T, K	3588	4137	4924	5589	6015	6324	6573	6785
Velocity, m/s	358	378	419	447	459	466	472	477
Atom mass fraction	9.179e − 2	0.1700	0.2222	0.2599	0.3027	0.3409	0.3971	0.4464
Density variation midpoint, cm	19.30	3.280	1.004	0.4762	0.3084	0.2349	0.1939	0.1703
N_2 1+ peak point, cm	0.7946	0.3105	0.1598	9.223e − 2	5.813e − 2	4.245e − 2	3.512e − 2	3.153e − 2

temperature calculation. However, the postshock equilibration process is predicted differently by the state-to-state method. There is a significant difference in the postshock equilibration process between the flow in the test section and the free-flight flow when p_0 is 100 atm. For $p_0 = 1000$ atm and for a large nozzle, the difference is small, signifying that the degree of simulation is good.

The accuracy of the present methodology is dictated mostly by that of the experimental data to which the state-to-state transition rate coefficients are adjusted. The only significant uncertainty the present methodology introduced is that of the linear interpolation of the correction factors [Eq. (5)]. If more is known about the state-to-state transition rates, this uncertainty can be removed.

Conclusions

The thermochemical nonequilibrium phenomena in air occurring in a shock tunnel are calculated by the state-to-state method. The result reproduces several features of the conventional two-temperature calculations. But it predicts the equilibration process behind the shock wave formed in the test section to be, in general, significantly different from that in free flight. Population of the upper vibrational states of N_2 is strongly affected by the interaction between N_2 and O. Presence of hydrogen atoms, originating from water vapor, can explain the fast vibrational equilibration observed in the past. For a large shock tunnel operating at 1000 atm, the calculation predicts that the free-flight condition is simulated fairly closely in the test section.

Acknowledgments

The author expresses sincere thanks to Igor Adamovich who supplied the forced harmonic oscillator model code and to Graham Candler for valuable discussions and encouragement.

References

[1] Holden, M. S., and Candler, G. V., "Experimental Studies in the LENS Shock Tunnel and Expansion Tunnel to Examine Real-Gas Effects in Hypersonic Flows," AIAA Paper 2004-0916, 2004.

[2] Nompelis, I., Candler, G. V., MacLean, M., Wadhams, T. P., and Holden, M. S., "Numerical Investigation of High Enthalpy Chemistry on Hypersonic Double-Cone Experiments," AIAA Paper 2005-584, 2005.

[3] Bender, D. J., "Measurement of Vibrational Population Distribution in a Supersonic Expansion of Carbon Monoxide," Ph.D. Thesis, Dept. of Mechanical Engineering, Stanford Univ., Stanford, CA, March 1975.

[4] Hurle, I. R., Russo, A. I., and Hal, J. G., "Spectroscopic Studies of Vibrational Nonequilibrium in Supersonic Nozzle Flows," *Journal of Chemical Physics*, Vol. 40, No. 8, April 1964, pp. 2076–2089.

[5] Park, C., "Estimation of Excitation Energy of Diatomic Molecules in Expanding Nonequilibrium Flows," *Journal of Thermophysics and Heat Transfer*, Vol. 9, No. 1, Jan.–March 1995, pp. 17–25.

[6] Bose, D., and Candler, G. V., "Thermal Rate Constants of the $N_2 + O \rightarrow NO + N$ Reaction Using *ab initio* $^3A''$ and $^3A'$ Potential Energy Surfaces," *Journal of Chemical Physics*, Vol. 104, No. 8, Feb. 1996, pp. 2825–2833.

[7] Bose, D., and Candler, G. V., "Thermal Rate Constants of the $O_2 + N \rightarrow NO + O$ Reaction Based on the $^2A'$ and $^4A'$ Potential Energy Surfaces," *Journal of Chemical Physics*, Vol. 107, No. 16, Oct. 1997, pp. 6136–6145.

[8] Adamovich, I. V., Macheret, S. O., Rich, J. W., and Treanor, C. E., "Vibrational Energy Transfer Rates Using a Forced Harmonic Oscillator Model," *Journal of Thermophysics and Heat Transfer*, Vol. 12, No. 1, Jan.–March 1998, pp. 57–65.

[9] Mansfield, D. K., Miles, R. B., Howard, P. J., Luff, J. D., Girgis, I. G., Brown, G. L., Lipinski, R. J., Pena, G. E., Schneider, L. X., Grinstead, J., and Howard, R., "Results of the 1 MW Radiatively-Driven Hypersonic Wind Tunnel Experiments," AIAA Paper 2004-1134, Jan. 2004.

[10] Allen, R. A., Rose, P. H., and Camm, J. C., "Nonequilibrium and Equilibrium Radiation at Super-Satellite Entry Velocities," AVCO-Everett Research Lab., Everett, MA, Rept. 156, Sept. 1962.

[11] Sharma, S. P., Ruffin, S. M., Gillespie, W. D., and Meyer, S. A., "Vibrational Relaxation Measurements in an Expanding Flow Using Spontaneous Raman Scattering," *Journal of Thermophysics and Heat Transfer*, Vol. 7, No. 4, Oct.–Dec. 1993, pp. 697–703.

[12] von Rosenberg, C. W., Bray, K. N. C., and Pratt, N. H., "The Effect of Water Vapor on the Vibrational Relaxation of CO," *Proceedings of the 13th Symposium (International) on Combustion*, Combustion Inst., Pittsburg, PA, 1971, pp. 89–98.

[13] Center, R. E., and Newton, J. F., "Vibrational Relaxation of N_2 by H_2O," *Journal of Chemical Physics*, Vol. 68, No. 8, April 1978, pp. 3327–3333.

[14] von Rosenberg, C. W., and Wray, K. L., "Vibrational Relaxation of CO by Fe-Atoms," *Proceedings of the 8th International Shock Tube Symposium*, Chapman and Hall, London, 1971, pp. 28.1–28.10.

[15] Perini, L. L., "Curve Fits of JANAF Thermochemical Data," Johns Hopkins Univ. Applied Physics Lab., Rept. ANSP-M-5, Silver Spring, MD, Sept. 1972.

[16] Millikan, R. C., and White, D. R., "Systematics of Vibrational Relaxation," *Journal of Chemical Physics*, Vol. 39, No. 1, Jan. 1963, pp. 98–101.

[17] Eckstrom, D. J., "Vibrational Relaxation of Shock-Heated N_2 by Atomic Oxygen Using the IR Tracer Method," *Journal of Chemical Physics*, Vol. 59, No. 6, Sept. 1973, pp. 2787–2795.

[18] Kiefer, J. H., and Lutz, R. W., "The Effect of Oxygen Atoms on the Vibrational Relaxation of Oxygen," *Proceedings of the 11th Symposium (International) on Combustion*, Combustion Inst., Pittsburgh, PA, 1967, pp. 67–76.

[19] Wray, K. L., "Shock-Tube Study of the Vibrational Relaxation of Nitric Oxide," *Journal of Chemical Physics*, Vol. 36, No. 10, May 1962, pp. 2597–2603.

[20] Taylor, R. L., Camac, M., and Feinberg, R. M., "Measurements of Vibration–Vibration Coupling in Gas Mixtures," *Proceedings of the 11th Symposium (International) on Combustion*, Combustion Inst., Pittsburg, PA, 1967, pp. 49–65.

[21] Hirschfelder, J. O., Curtiss, C. F., and Bird, R. B., *Molecular Theory of Gases and Liquids*, Wiley, New York, 1963, pp. 1126–1127.

[22] McLaren, T. I., and Appleton, J. P., "Shock-Tube Measurements of the Vibration–Vibration Energy Exchange Probability for the CO–N_2 System," *Proceedings of the 8th International Shock Tube Symposium*, edited by J. L. Stollery, A. G. Gaydon, and P. R. Owen, Chapman and Hall, London, 1972, pp. 27.1–27.9.

[23] Baulch, D. L., Drysdale, D. D., and Horne, D. G., "Evaluated Kinetic Data for High Temperature Reactions," *Homogeneous Gas Phase Reactions of the* H_2–N_2–O_2 *System*, Vol. 2, CRC Press, Cleveland, OH, 1973.

[24] Baulch, D. L., Drysdale, D. D., Duxbury, J., and Grant, S. J., "Evaluated Kinetic Data for High Temperature Reactions," *Homogeneous Gas Phase Reactions of the* O_2–O_3 *System,* CO–O_2–H_2 *System, and of Sulphur-Containing Species*, Vol. 3, Butterworths, London, 1976.

[25] Appleton, J. P., Steinberg, M., and Liquornik, D. J., "Shock-Tube Study of Nitrogen Dissociation Using Vacuum-Ultraviolet Light Absorption," *Journal of Chemical Physics*, Vol. 48, No. 2, Jan. 1968, pp. 599–608.

[26] Park, C., *Nonequilibrium Hypersonic Aerothermodynamics*, Wiley, New York, 1989.

[27] Sharma, S. P., and Gillespie, W., "Nonequilibrium and Equilibrium Shock Front Radiation Measurements," *Journal of Thermophysics and Heat Transfer*, Vol. 5, No. 3, July–Sept. 1991, pp. 257–265.